Depolymerization of Double-Stranded Xanthan by Acid Hydrolysis: Characterization of Partially Degraded Double Strands and Single-Stranded Oligomers Released from the Ordered Structures

Bjørn E. Christensen,*,† Olav Smidsrød,† Arnljot Elgsaeter,‡ and Bjørn T. Stokke‡

Norwegian Biopolymer Laboratory, Department of Biotechnology and Department of Physics and Mathematics, University of Trondheim, NTH, N-7034 Trondheim, Norway

Received June 2, 1993; Revised Manuscript Received August 9, 1993•

ABSTRACT: Double-stranded xanthan was depolymerized by partial acid hydrolysis to produce samples where M_w ranged from 6×10^6 to 7×10^4. These were characterized with respect to chemical composition in the side chains, molecular weight (light scattering), molecular weight distribution (HPLC, gel filtration), intrinsic viscosity, and conformation (optical rotation). Additional information about molecular size and conformation was obtained by electron microscopy. For each sample a fraction consisting of depolymerized, double-stranded species could be obtained. Their conformational properties were largely analogous to undegraded xanthan, despite the reduced M_w and the changes in the side chains. The chain flexibility increased with degradation time, as indicated by a gradual reduction in persistence length (q), calculated from electron micrographs and from the $[\eta]$–M_w relationship using the wormlike chain model. As the degradation proceeded, a second fraction, consisting of shorter and conformationally *disordered* fragments, constituted a progressively larger part of the population. This is in accordance with the model requiring the minimum chain length (DP_{min}) to take part in an ordered, double-stranded structure in a cooperative manner. Their release partly explains the increased flexibility of the remaining double-stranded species, since their release exposes local single-stranded and hence more flexible, regions. The experimental M_w data are in qualitative accordance with a Monte Carlo model for the apparent depolymerization kinetics of double-stranded polymers. The model also predicts a relationship between M_w and the amount of disordered fragments which depends on DP_{min}. Comparison to experimental data gives a minimum estimate of DP_{min} in the range of 10–15 glucose residues.

Introduction

The polysaccharide xanthan (Figure 1) is used industrially in a wide range of applications,[1] which usually take advantage of the large viscosifying power of xanthan molecules when they occur in a stiff and extended ordered conformation. Xanthan may also form gels, either in the presence of trivalent cations like Cr(III)[2–5] or by utilization of its ability to interact with galactomannans.[6,7] The nature of the ordered and disordered states of xanthan has been a matter of debate for many years. Recent work in several laboratories suggests, however, that ordered xanthan occur as double helices in the solid state[8] and as double-stranded species,[9–17] probably very similar to the double helices,[11] also in solution.

Partially hydrolyzed xanthans[18,19] represent a novel family of polymers with different chemical compositions. Following the rapid hydrolysis of pyruvate and acetate substituents, preferential hydrolysis of the terminal β-mannose in the side chains gives rise to a series of high molecular weight xanthan variants approaching the "polytetramer". Such variants were first reported to be produced through genetic engineering of xanthan-producing bacteria.[20] In addition, some hydrolysis of the inner α-mannose gives rise to regions in the backbone devoid of side chains. Despite such chemical heterogeneity, it has been shown[19] by optical rotation and differential scanning calorimetry (DSC) that these polymers still display the typical temperature-driven, salt-dependent cooperative conformational transition, irrespective of the changes in the side chains. However, the magnitude of the optical rotation and the transition enthalpy (ΔH_{cal}) is strongly and linearly dependent upon the content of β-mannose. On the other hand, the transition temperature (T_m) is essentially independent of the degree of hydrolysis, and calculation of the Zimm–Bragg cooperativity parameter σ indicated a larger degree of cooperativity (lower σ values) with increasing extents of hydrolysis. This is opposite of what might be expected when only considering the effect of reducing the chain length. We were encouraged by these findings to pursue the investigations of the properties of hydrolyzed xanthan, with emphasis on the nature of the ordered and disordered conformations in solution. Such investigations may prove an alternative route toward an increased understanding of the ordered conformation of xanthan.

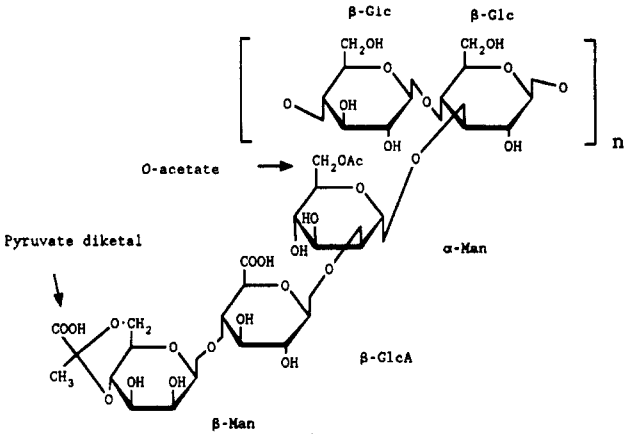

Figure 1. Pentasaccharide repeating unit of xanthan. Abbreviations: β-Glc, β-D-glucose; β-GlcA, β-D-glucuronic acid; α-Man, α-D-mannose; β-Man, β-D-mannose.

* Author to whom all correspondence should be addressed.
† Department of Biotechnology.
‡ Department of Physics and Mathematics.
• Abstract published in *Advance ACS Abstracts*, October 1, 1993.

0024-9297/93/2226-6111$04.00/0

The first part of this work is therefore focused on a macromolecular characterization of partially hydrolyzed xanthans, in the ordered state, using low-angle laser light scattering (LALLS) which yields the weight-average molecular weight (M_w) and the osmotic second virial coefficient (A_2'). These data are then used in combination with intrinsic viscosity data to obtain the parameters in the Mark–Houwink–Sakurada equation. The persistence length (q) and linear mass density (M_L) are further obtained according to the wormlike chain model. In these analyses the chemical composition enters as an additional variable, and distinctions are made between the effects due to changes in the equivalent weight of the repeating unit and effects due to changes in chain length and flexibility. Additional information is obtained by electron microscopy, which independent of the previous measurements yields conformation parameters such as q and M_L, as well as direct observation of the strandedness.[14-17]

The second part of this study is concerned with an analysis of the depolymerization kinetics, which is expected to be strongly dependent upon the strandedness of multiple-stranded polymers. When subjected to random depolymerization of the polymer backbones, such polymers initially show only marginal reduction in the measured molecular weight, because of stabilizing forces between the strands.[21] A total break in the multiple-stranded structure then only occurs when each of the individual strands are broken in positions which are not separated by more than a certain critical distance along the chain. This distance, DP_{min}, corresponds to the minimum number of monomers (i.e., sugar residues in the backbone) needed to maintain a multiple-stranded structure. The initial phase is followed by a transition to a second time domain with apparently more rapid molecular weight decay, due to concomitant disintegration of multiple-stranded fragments upon further depolymerization of the individual polymer chains. This effect has also been demonstrated in the enzymatic degradation of double-stranded DNA.[22] Viscometric studies of the degradation kinetics of xanthan[18,23,24] have indicated significant deviations from what might be expected if ordered xanthan were single-stranded species in solution. By means of a Monte Carlo simulation,[21] we have shown that in a random depolymerization process the strandedness is directly manifested in the time dependence of the molecular weight decay in the second time domain through the exponent υ, as given in eq 1:

$$M_w(t)/M_w(t=0) = kt^{-\upsilon} \quad (1)$$

The parameter υ was found to be 2.3 (±0.1) for a triple-stranded polymer, 1.66 (±0.06) in the double-stranded case, and 1 (as expected) for single strands, provided that (DP_{min}) was below 15. Application of eq 1 to partially hydrolyzed xanthan where M_w values were estimated from [η] data[21] gave strong support for the double-stranded model. The simulations[21] also predicted that disordered low molecular weight frgaments (oligomers) should be released from the main chain of a double-stranded, ordered structure. This should occur when the distance between two hydrolyzed bonds in the same strand became too short to stabilize the fragment in an ordered structure associated with the other strand. The maximum possible length of such released and disordered fragments should therefore provide information about the parameter DP_{min}. Likewise, experimental data on the relative content of the low molecular weight disordered fragments can be used in combination with the simulations to estimate DP_{min}. High-performance liquid chromatography (HPLC) and gel filtration methods are therefore developed to isolate and analyze these fragments. Supporting information is obtained by chiroptical measurements. The depolymerization is also followed by monitoring the formation of reducing ends and the liberation of glucose from the backbone.

Experimental Section

Samples. Modified xanthans were prepared from Keltrol lot no. 21322A (food-grade xanthan, Kelco Division of Merck) by hydrolysis in 0.1 N HCl at 80 °C as described earlier.[18,19] At this pH the transition temperature is well above 100 °C, ensuring that the hydrolysis took place when the samples were in the ordered state.[18] Following hydrolysis the samples were cooled to ambient temperature and neutralized by adding aqueous NaOH to a final pH of 6–7. The more degraded samples were then concentrated under reduced pressure until they became as viscous as the undegraded samples. A major portion of each sample was dialyzed extensively against MQ water at 4 °C in order to remove excess salts and low molecular weight degradation products. The latter includes mono-, di-, and trisaccharides released from the side chains as well as fragments of similar size originating from the glucan backbone. Larger oligomeric fragments (DP ≥ 4) are nondialyzable.[25] Dialyzed stock solutions (3–5 mg mL^{-1}) were stored at 4 °C before further analysis. Aliquots of the dialyzed samples were freeze-dried, which afforded the determination of the polymer concentration in the stock solutions. Concentrations were alternatively calculated from the carbon content, as measured on a carbon analyzer (Carlo-Erba Model NA 1500).

Chemical Analyses. Analysis of the sugar composition by gas–liquid chromatography following methanolysis and trimethylsilylation was performed as described earlier.[18] More consistent results from this analysis were obtained by mixing the xanthan (approximately 100 μg in 0.5 mL of water) with the internal standard (*myo*-inositol, 10 μg) and freeze-drying the mixture directly in the vials used for subsequent methanolysis, rather than using previously freeze-dried samples. The reason is probably that a larger fraction of the sample, which is initially insoluble in methanolic HCl, is exposed to the methanolytic agents in the former case. The content of free glucose in undialyzed samples was analyzed enzymatically using a commercial kit (Boeringer Mannheim; catalogue no. 716 251). Reducing sugar was analyzed by the Nelson reagent method[29] and by the dinitrosalicylic acid (DNS) reagent method.[30] Uronic acids were measured by the sulfamate/*m*-hydroxydiphenyl/sulfuric acid assay.[31] Total carbohydrate was measured by the phenol/sulfuric acid method.[32]

Optical Activity Measurements. These were performed as previously described.[18,19]

Low-Angle Laser Light Scattering (LALLS) Measurements. These were performed on a Chromatix KMX-6 light scattering photometer. The refractive index increment (dn/dc) was taken to be 0.15.[26] Although dn/dc may depend upon the chemical decomposition of a polysaccharide,[27] we observed a strict linear relationship, independent of the chemical composition of the side chains, between the amount of injected polysaccharide and the area under the refractive index curve observed in the HPLC–LALLS experiments (see below). This finding indicates[27] that dn/dc does not depend on the composition of the side chains in partially hydrolyzed xanthans. Light scattering analyses were performed directly on dialyzed solutions of hydrolyzed polysaccharide, avoiding a dissolution step, as well as on freeze-dried samples subsequently dissolved in pure water. In the latter case the sample concentrations were chosen so that the ordered conformation was maintained (see Results). Following the addition of NaCl and dilution to the desired concentration, the solutions were filtered before light scattering measurements, using pore sizes of 0.8 μm for samples 1 and 2, 0.45 μm for samples 3–8, and 0.22 μm for samples 9–13. Samples were introduced to the measuring cell by means of a peristaltic pump (flow rate approximately 75 μL min^{-1}), with a second in-line filter using the same filter type as in the first filtration. Analyses of the carbohydrate content showed that no material was removed by the filtration.

Table I. Characteristics of the Samples

				static light scattering measurements							
				0.1 M NaCl (not freeze-dried)		0.1 M NaCl (freeze-dried)		0.005 M NaCl (freeze-dried)		HPLC with	
sample	hours	$f_{\beta\text{-Man}}$	f_{ABA}	M_w (×10^{-3})	A_2' (×10^4)	M_w (×10^{-3})	A_2' (×10^4)	M_w (×10^{-3})	A_2' (×10^4)	0.1 M NaCl: M_w (×10^{-3})	$[\eta]$ (mL/g)
1	0	1.00	1.00	6500	4.2						2100
2	3	0.92	0.99	2900	7.8						1600
3	22	0.52	0.95	2000	5.0						1400
4	31	0.40	0.93	1200	4.0						1200
5	40	0.31	0.90	1200	5.1						1400
6	50	0.23	0.88	1200	6.1	1400	7.9	1200	32		1500
7	62	0.16	0.86	970	7.3	1000	3.9	980	30		1300
8	79	0.10	0.82	630	8.6	710	6.3	710	40	640	1000
9	100	0.05	0.78	510	8.0	580	7.8	560	42	540	870
10	126	0.02	0.73	390	8.9			610	44	440	700
								590	31	420	
11	159	0.01	0.67	280	9.2			380	54	340	530
								350	32	270	
12	199	0.00	0.61	190	9.7			260	49	250	390
								250	51	240	
13	247	0.00	0.54	62	7.8			77	51	72	140
								72	37	74	

HPLC–LALLS. Analytical HPLC–LALLS experiments were performed using two serially connected columns (TSK G6000-PWXL and TSK G5000-PWXL) and eluted (Spectra-Physics IsoChrom LC pump, 0.4 mL min^{-1}) at ambient temperature with 0.1 M NaCl. Injection volumes were 50 or 100 μL with polysaccharide concentrations in the range 0.6–4 mg mL^{-1}. Light scattering data (Chromatix KMX-6 light scattering photometer equipped with the standard HPLC flow cell) and refractive index data (Shodex RI SE-61 detector) were collected and analyzed by PCLALLS software, which also controlled the autoinjector (Shimadzu SIL-10A).

Gel Filtration. Preparative gel filtration was performed on a column (2.6 × 80 cm) of Sephacryl S-100 HR, equilibrated and eluted at 25 mL h^{-1} with 0.1 M NaCl. The elution was monitored using a refractive index detector (Shimadzu RID-6A). Fractions (8.3 mL) were analyzed for total carbohydrate, uronic acids, and reducing ends as described above. Pooled fractions were dialyzed against distilled water and freeze-dried.

Viscosity Measurements. These were carried out in a capillary viscometer system (Scott-Geräthe no. 531 01/0A with AVS 310 controller) with PC-controlled data acquisition and instrument control, including sequential dilution with solvent. Intrinsic viscosities were determined according to Huggin's and Kraemer's equations as described earlier.[28]

Enzymatic Depolymerization. Depolymerization by cellulase was performed in salt-free polysaccharide solutions at 50 °C, using Cellulysin (Calbiochem; 2 μg of enzyme per mg of polysaccharide).

Electron Microscopy. Preparation of replicas for electron microscopy was carried out as described earlier.[14-16,33] Aliquots of the aqueous xanthan samples selected for electron microscopic characterization were diluted with 1.0 M NH_4Ac (ammonium acetate) and 60% glycerol to a final polymer concentration of 5–20 μg mL^{-1} in 0.1 M NH_4Ac and 50% glycerol. The volatile buffer was omitted in some preparations in order to induce the disordered conformation of xanthan. A total of 50 μL of these diluted samples was sprayed onto freshly cleaved mica disks, vacuum dried at 10^{-6} Torr, T = 20 °C for 60 min. The dried specimens were subsequently replicated while rotated with 0.6–0.8 nm of Pt from an angle of 6° and 8–10 nm of C from an angle of 90°. The electron micrographs were obtained using a Philips EM 400T electron microscope at a nominal electron optic magnification 17 000–60 000 times. The calibration of the magnification of the final printed micrographs was carried using a line grid (1200 lines mm^{-1}; Agar Aids). The dimensions and flexibility of the xanthan chains thus visualized were digitized and analyzed as described previously.[16,34]

Results

Figure 2 shows the changes in sugar composition of xanthan upon hydrolysis at 80 °C in 0.1 M HCl in the presence of 10 mM NaCl, followed by extensive dialysis to remove the mono–, di–, and trisaccharides which could be released from the side chains, as well as salts. These results are in line with previous data[18] and demonstrate the preferential hydrolysis of the terminal β-mannose and a slower hydrolysis of the inner α-mannose, whereas the linkage between the glucuronic acid and the α-mannose is resistant to hydrolysis.[18] Hydrolysis of the α-mannose therefore releases an aldobiuronic acid (D-GlcA*p*-β-(1→2)-D-Man*p*), abbreviated as ABA in the following. By fitting the experimental data to two independent first-order rate processes, rate constants of 0.027 and 0.0025 h^{-1} were obtained for the hydrolysis of β- and α-mannose, respectively. From these numbers the calculated compositions corresponding to 13 different hydrolysis times, expressed as fractions of β-mannose ($f_{\beta\text{-Man}}$) and aldobiuronic acid (f_{ABA}), are given in Table I. Note that f_{ABA} also includes the ABA units that have an β-mannose linked to it. The samples range from intact xanthan to variants containing no β-mannose and where the content of ABA is reduced by 46%. Note also that none of the samples except for the unmodified xanthan contain pyruvate and acetate, which are hydrolyzed rapidly under the conditions used here.[18]

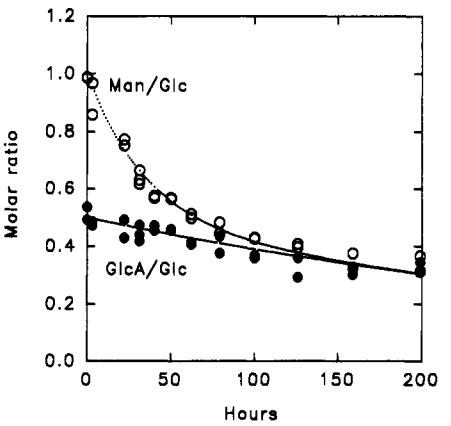

Figure 2. Change in sugar composition (molar ratios relative to glucose) in the nondialyzable fraction upon hydrolysis of xanthan in 0.1 M HCl at 80 °C. The lines were obtained by fitting the experimental data (○, ●) to two independent first-order rate constants for the hydrolysis of the β-mannose and the aldobiuronic acid, respectively (see text).

Figure 3 shows the specific optical rotation, calculated as the rotation per cellobiose unit in the backbone, $[\alpha]_{Glc2}$,[19]

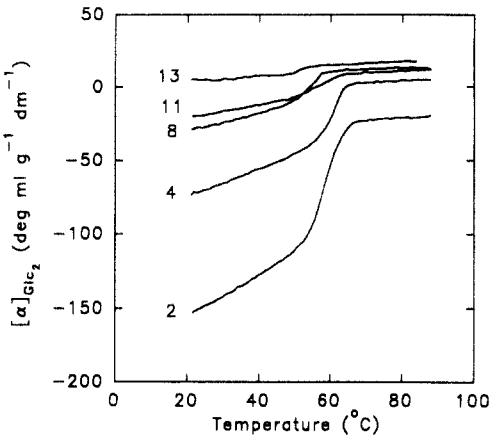

Figure 3. Specific optical rotation (365 nm) per cellobiose residue, $[\alpha]_{Glc2}$, versus temperature for some of the partially hydrolyzed xanthans. The ionic strength is 10 mM. More information about the samples is given in Table I.

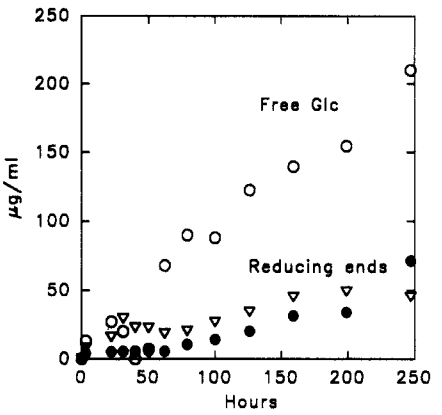

Figure 4. Formation of reducing ends (●, ▽) in the nondialyzable fraction and liberation of free glucose monomer (○) (undialyzed samples) upon hydrolysis of xanthan in 0.1 M HCl at 80 °C. Reducing ends were analyzed by the Nelson[29] method (●) and the disalicylic acid reagent[30] (▽) using glucose as standard.

versus temperature in 10 mM NaCl for samples 2, 4, 8, 11, and 13. The data conform well with previous data,[19] showing the characteristic cooperative order–disorder transition near 60 °C at this ionic strength. The increase in $[\alpha]_{Glc2}$, particularly in the ordered state, for the more extended hydrolysis times is ascribed to the selective removal of β-mannose.[18,19] The midpoint of the transition, T_m, decreases only slightly with the depolymerization time, and at I = 10 mM all samples appear to be in the ordered conformation at room temperature. It was also of interest to test whether it was possible to prepare salt-free solutions of xanthan at room temperature without inducing a conformational transition. This is the preferred procedure for preparing samples for light scattering measurements[35,36] with a minimum amount of aggregates. At a concentration of 3.72 mg mL^{-1} the onset of a detectable transition for sample 12 occurred at approximately 28 °C, and T_m was 40.2 °C. Sample 11 (4.27 mg mL^{-1}) showed essentially the same curve (data only up to 43 °C, precluding an accurate determination of T_m). Lowering the concentration of sample 11 to 1.74 mg mL^{-1} (corresponding to a decrease in calculated ionic strength due to the glucuronic acid from 5.1 to 2.1 mM) shifted the transition curve 10 °C downward, showing an onset of a transition at approximately 20 °C. It was also found that upon addition of HCl to 10 mM (at 1.66 mg mL^{-1}) sample 11 was in the ordered state at all temperatures investigated (10–90 °C), confirming that the hydrolysis occurred entirely under conditions where the xanthans were in the ordered state.

Table I gives the weight-average molecular weights (M_w) of the hydrolyzed xanthans, measured in 0.1 M NaCl by LALLS. The samples were prepared by adding NaCl (twice the final concentration) to equal volumes of dialyzed solutions of polysaccharide (>2 mg mL^{-1}) to a final NaCl concentration of 0.1 M, followed by dilution with 0.1 M NaCl to the desired polymer concentration. The results demonstrate that M_w decreases for increasing hydrolysis times. However, in accordance with previous data on $[\eta]$,[18] M_w remains remarkably high.

Table I also gives the osmotic second virial coefficient (A_2') in 0.1 M NaCl. Values in the range of (4–9) × 10^{-4} (mL mol g^{-2}) are close to or slightly higher than those oberved for sonicated xanthans in the same solvents.[12,13,35,36]

When dissolved in 5 mM NaCl, essentially the same M_w values as in 0.1 M NaCl are obtained. An exception is sample 10, which in these measurements seems to deviate. As expected for a polyelectrolyte, A_2' becomes much larger when the ionic strength is reduced from 0.1 M to 5 mM. Values near 5 × 10^{-3} mL g^{-2} were observed, in accordance with values found for a sonicated xanthan in the same solvent.[35,36]

Table I further gives the experimentally determined intrinsic viscosities of the samples in 0.1 M NaCl, showing a decrease with increasing hydrolysis times, in line with earlier data[18] and the M_w data. It should be noted that for $[\eta]$ > 1000 mL g^{-1} the observed $[\eta]$ values do not correspond to zero shear rate intrinsic viscosities due to the relatively high shear rate in the capillary viscometer.

Since acid hydrolysis of polysaccharides leads to the formation of reducing ends, it was also of interest to attempt a quantitative determination of the content of reducing ends, particularly in the *non*dialyzable fraction. Data from the end-group analyses, expressed as glucose equivalents, are shown in Figure 4. The results, which should not include the smallest fragments, e.g., mono-, di-, and trisaccharides liberated from the side chains, show an increase in the content of detectable reducing ends. The rate of formation of reducing ends seems to increase after 50–70 h.

As a consequence of the acidic hydrolysis a small amount of free glucose was expected to be present in the *undialyzed* reaction mixture following hydrolysis. The data from the enzymatic analysis of free glucose in undialyzed samples are also shown in Figure 4, which demonstrate a nearly linear increase in the content of free glucose with increasing hydrolysis time.

Figure 5 shows the HPLC elution profiles of samples 5–13 (nondialyzable fraction), all obtained at room temperature in 0.1 M NaCl. The high molecular weight samples essentially display a single peak (designated A) near the void volume of the columns, with calculated M_w values in accordance with the data obtained by static light scattering. Peak D contains mainly salt since it becomes negative when the injected sample has a slightly lower salt content than the eluent. The more degraded samples show in addition two major peaks (B and C). The relative areas of the latter peaks appear to increase with increasing hydrolysis times. These peaks yield very low intensities of scattered light in the HPLC–LALLS experiments (not shown in Figure 5), precluding an estimation of the molecular weight. The elution volume of peak C is within the range observed for pullulan standards with number-average molecular weights (M_n) of 8000.

Semipreparative gel filtration experiments on a column of Sephacryl S-100 were performed in order to isolate larger amounts of the oligomeric fragments seen in the HPLC. The elution profiles for sample 13 is shown in Figure 6a.

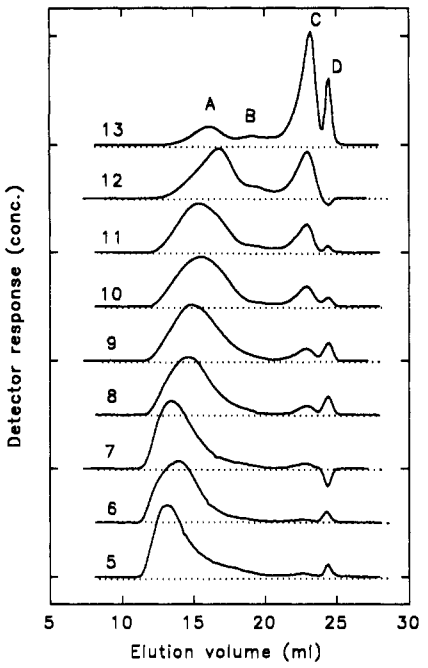

Figure 5. HPLC elution profiles (refractive index detector) of samples 5–13. Solvent: 0.1 M NaCl.

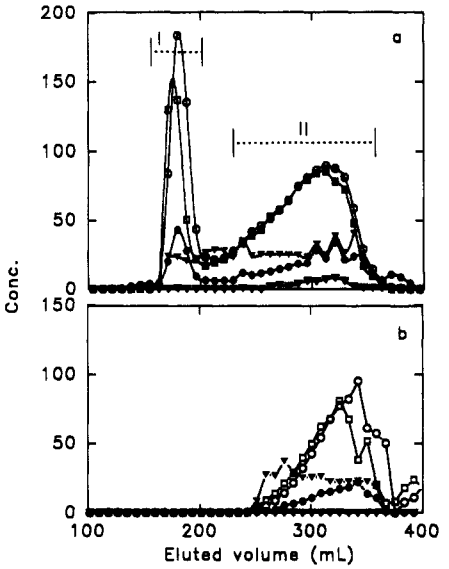

Figure 6. Gel filtration of sample 13 (a) and fraction II following depolymerization with cellulase (b). Fractions were assayed for total carbohydrate (○), uronic acids (●), reducing ends (▽), and refractive index (□). Symbol ▼ is the calculated ratio (×100) between uronic acids and total carbohydrate.

The elution curve corresponds to the analytical HPLC results, with one peak in the void volume and a well-separated peak at larger elution volume. The fractions were analyzed for total carbohydrate, uronic acids, and reducing ends, in addition to continuous monitoring of the refractive index. All analyses reveal the same peaks. The most significant observation is a constant ratio (0.26 ± 0.04) between uronic acids and total carbohydrate. This shows that all fragments must have the same chemical composition. The low sensitivity of the analyses of reducing ends precluded a reasonably accurate quantification of reducing ends, except in the low molecular weight fraction, where the presence of reducing ends is clearly seen.

The eluates corresponding to fraction II in Figure 6a were pooled, dialyzed to remove the salts, and freeze-dried. A solution of 5 mg in 1.5 mL of water was heated to 50 °C

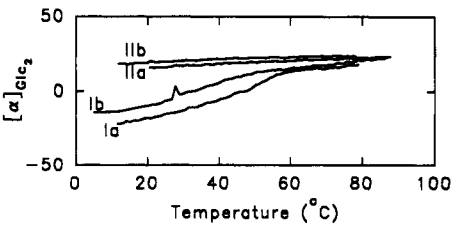

Figure 7. Specific optical rotation per cellobiose residue, $[\alpha]_{Glc2}$, versus temperature for fractions I and II in Figure 6a. Measurements were performed in 10 mM NaCl (Ia, IIa) and in pure water (Ib, IIb).

Table II. Results from Electron Microscopic Analyses

sample	$M_w \times 10^{-6}$	L_n (nm)	L_w (nm)	n	M_L (nm^{-1})	q_{2D}	q_{3D}[a]
2	2.88	850	1560	149	1850	58	93 ± 11
7	0.97	336	645	191	1500	25	40 ± 5
8	0.63	274	470	212	1340	26	42 ± 5

[a] Calculated from q_{2D} by correcting for sample dimensionalities of 2.6 ± 0.2 in the electron micrographs.[34]

to induce the disordered conformation, and cellulase (10 μg) was added. The sample was incubated for 48 h and then cooled. NaCl was added to a final concentration of 0.1 M, and the sample was subjected to gel filtration as described above. The resulting elution curve is shown in Figure 6b. The elution profile is generally shifted toward higher elution volumes, indicating that the sample has been depolymerized by cellulase.

The conformational properties of the high and low molecular weight fractions isolated from sample 13 by gel filtration were examined by optical rotation. Figure 7 shows the temperature dependency of the specific optical rotation ($[\alpha]_{Glc2}$) for both samples. The data clearly demonstrate that the high molecular weight fraction in 10 mM NaCl undergoes the characteristic conformational transition, with an estimated T_m near 50 °C, in accordance with the unfractionated sample 13 (Figure 3). In distilled water T_m is reduced by approximately 10 °C at a polymer concentration of 1.1 mg mL^{-1}. The low molecular weight fraction is, on the other hand, disordered at all temperatures, both in distilled water and in 10 mM NaCl. These data show that for extensively degraded samples $[\alpha]_{Glc2}$ at temperatures below T_m is increased not only due to the loss of β-mannose but also due to an increase in the content of disordered, low molecular weight fragments.

Figure 8 shows electron micrographs of some of the partially hydrolyzed xanthan samples. The overall impression is that the least degraded samples appear with polymeric shapes resembling the intact xanthan ("polypentamer"). The typical appearance of a rather stiff chain is observed when the preparation started from the ordered conformation. For the most degraded sample, an additional fraction of small species distinct from the background is observed (Figure 8d).

Figure 9 shows histograms of contour lengths, and Table II lists the number- and weight-average contour lengths, L_n and L_w, respectively, for the samples selected for electron microscopy. These data show that there is a reduction of average chain lengths as the hydrolysis proceeds. The linear mass density M_L, calculated as the ratio between the experimentally determined M_w and L_w, is also observed to decrease for prolonged hydrolysis times. This is in qualitative agreement with the expected loss of mass due to hydrolysis and removal of residues from the side chains.

The observed trajectories of the polysaccharide chains are also used to determine the chain stiffness by deter-

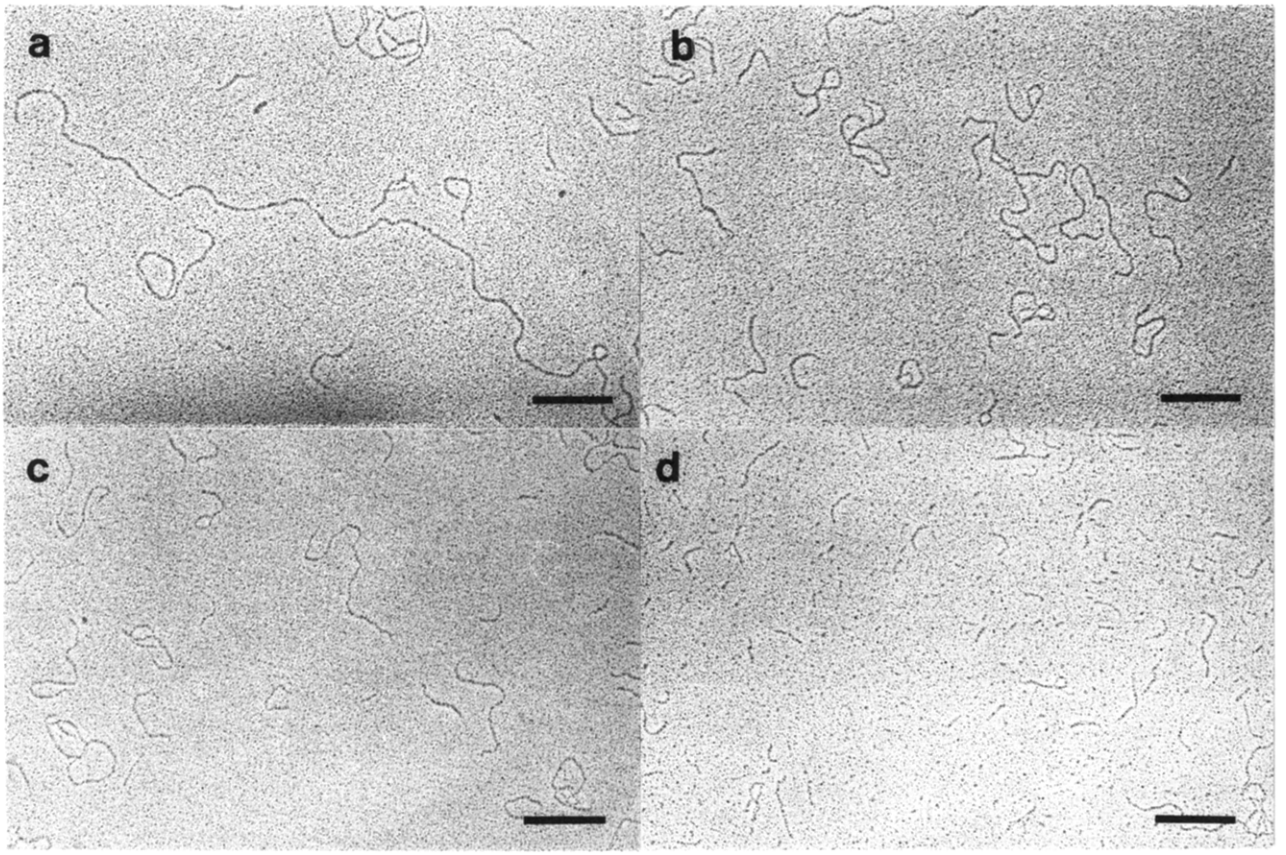

Figure 8. Electron micrographs of samples 2 (a), 7 (b), 8 (c), and 13 (d), all prepared in 0.1 M NH_4Ac, preserving the ordered conformation. Scale bar: 200 nm.

Table III. Transition Temperature in the Presence of Glycerol

salt	glycerol (%)	T_m (°C)
10 mM NaCl		53.0
10 mM ammonium acetate	20	51.6
10 mM ammonium acetate	60	48.4
20 mM ammonium acetate	20	61.1
20 mM ammonium acetate	60	64.1

mining the change in the tangential direction (θ) as a function of the contour distance l, according to the method described previously.[16,34] The approach predicts for the strictly two-dimensional case that the average $\langle\theta(l)\rangle = 0$ and that $\langle\theta^2(l)\rangle = l/q_{2D}$, where q_{2D} is the apparent persistence length observed from these two-dimensional micrographs. Methods to correct the observed q_{2D} for systematic differences in an apparent dimensionality to the solution-state value, q_{3D}, are described earlier.[34] The experimentally determined $\langle\theta^2(l)\rangle$ for three xanthan samples (Figure 10) shows that $\langle\theta^2(l)\rangle$ is linear up to at least 6–7 times the apparent q_{2D}. The calculated q_{3D} values (Table II) indicate a decrease in the chain stiffness parameter for increasing degrees of hydrolysis.

As with undegraded xanthans, preparation for electron microscopy in the absence of NH_2Ac induces partial or complete strand separation of the double-stranded structures into single strands. Electron micrographs for some of the samples prepared in this way are shown in Figure 11.

The temperature dependence of the optical rotation in the presence of glycerol was also investigated, since aqueous glycerol is used as solvent when preparing samples for electron microscopy. A depyruvated and deacetylated sample, ultrasonically depolymerized to $[\eta] = 980$ mL g^{-1}, was used in this case. The data are given in Table III and suggest that glycerol does not have a major influence on T_m and that the ionic strength is the most important factor controlling T_m also in this solvent.

Discussion

Partially hydrolyzed xanthans represent a family of polymers which is heterogeneous with respect to both chemical composition and molecular size. A range of physical properties more or less similar to those of intact xanthan may thus be expected. The origin of the observed changes in conformational properties may be expected to be difficult to elucidate when so many parameters change simultaneously and independently. It turns out, however, that all variants investigated carry with them some characteristic features of native xanthan which do not depend significantly on chemical composition. In the following discussion we will aim at distinguishing between the basic properties that are conserved upon partial hydrolysis and those effects that pertube the initial properties because of changes in the chemical structure of the side chains, as well as the conformation and strandedness of the glucan backbone.

It has already been demonstrated[19] that with respect to the chiroptically or calorimetrically observed conformational transition the partially hydrolyzed xanthans behave qualitatively similar to undegraded xanthan, irrespective of the composition of the side chains. In spite of this, there are changes in the quantitatively determined optical rotation as well as the transition enthalpy which depends largely, but not solely, on the composition of the side chains. The working model is therefore that the double-stranded conformation is conserved during the hydrolysis and that the double-to-single-stranded conformational change may take place in all cases, depending on ionic strength and pH as in native xanthan.

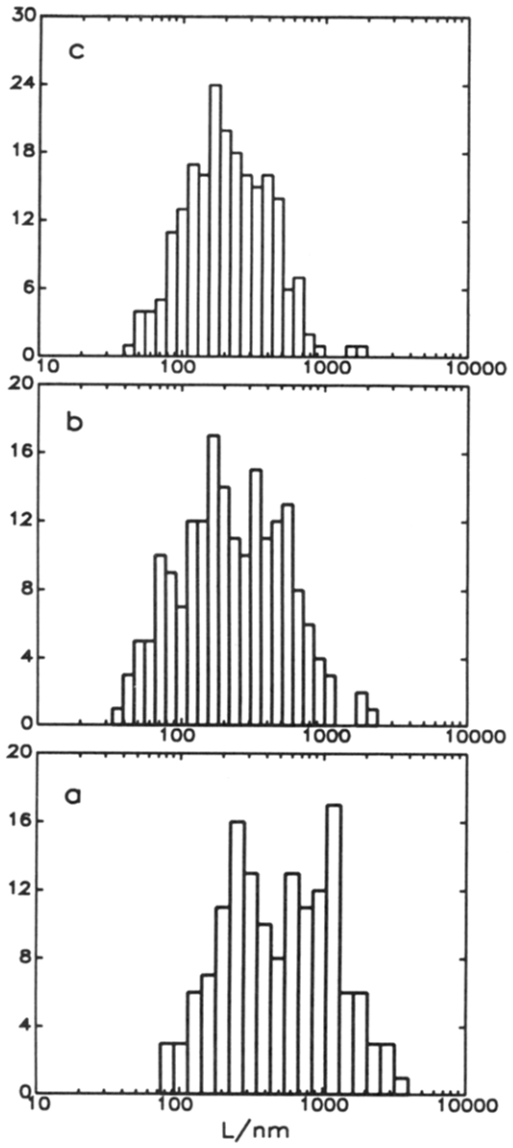

Figure 9. Contour length distributions observed in electron micrographic preparations of samples 2 (a), 7 (b), and 8 (c).

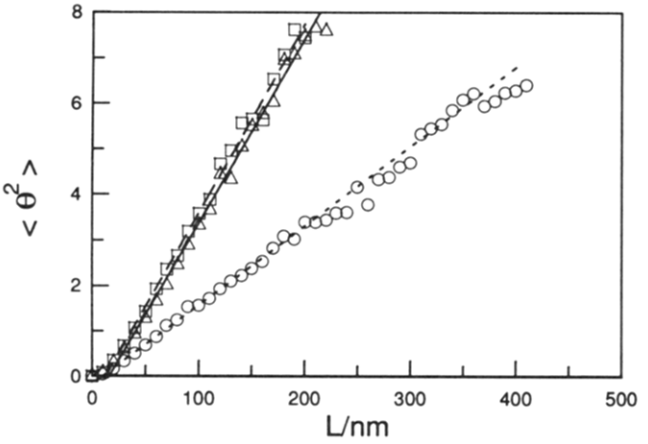

Figure 10. $\langle \theta^2 \rangle$ vs L for samples 2 (○), 7 (△), and 8 (□).

The electron micrographs of partially hydrolyzed xanthan confirm this picture. Despite the substantial changes in the side chains, the basic double-stranded conformation is maintained when the samples are in the ordered state. When exposed to disordering conditions (salt-free solutions at very low concentrations), extensive splitting into more flexible single chains is observed. These results are entirely

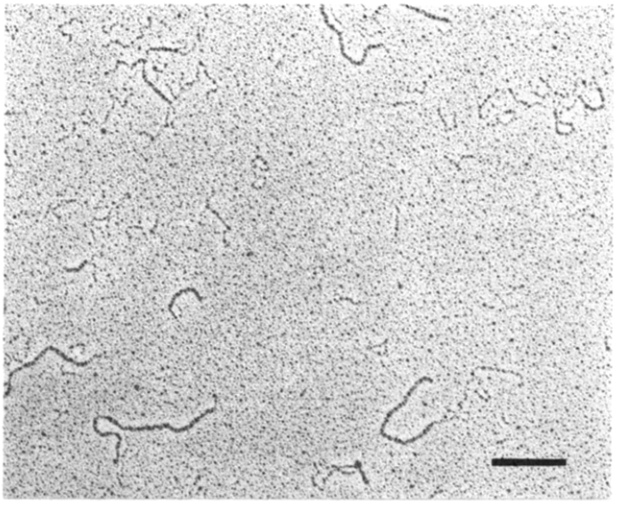

Figure 11. Electron micrographs of sample 3 prepared in the absence of NH_4Ac in order to induce the disordered, single-stranded conformation. Scale bar: 200 nm.

in line with the working hypothesis, as well as previous results obtained with unhydrolyzed xanthans.[14-17]

This conclusion is also corroborated by the present finding of a linear mass density for the least degraded sample, M_L = 1850 nm^{-1} (Table II), which is consistent with that reported previously for double-stranded xanthan.[14-17] We would like to emphasize that M_L is here obtained as the ratio between two experimentally determined parameters which are the same type of average. A reduction in linear mass density is observed as the hydrolysis proceeds (Table II). Both the side-chain truncation and release of oligomeric species are potential sources for this decrease. The released oligomeric fragments will most likely appear with a very small extension in the electron micrographs due to their low molecular weight and single-strandedness and were therefore not taken into account in the digitalization. The side-chain truncation was therefore considered as the major source of the observed reduction in M_L. In fact, using the apparent molecular weight M_w' (eq 2), it is found that $M_L' = M_w'/L_w$ = 1920 and 1780 nm^{-1} for samples 7 and 8, respectively. In view of the 10% relative error in M_L[16] and the previously reported variation in M_L for various xanthan samples,[15] this suggests that side-chain truncation is the origin of the observed reduced M_L even for extended hydrolysis times.

Determination of chain stiffness based on the observed chain trajectories in the electron micrographs indicates a reduced persistence length from q_{2D} = 58 nm to q_{2D} = 25 nm for initial to the most hydrolyzed samples (Table II). The value observed for the initial situation is close to that reported previously for intact double-stranded xanthan,[34] whereas the latter values conform with that reported for single-stranded xanthan.[34] The reduction in chain stiffness most likely arises from scissions of individual strands of the double-stranded structure. The number of scissions, and subsequent release of oligomeric fragments, is envisaged to be eventually so large that the chain effectively behaves as a single-stranded structure. Corrected for the apparent sampling dimensionality yields persistence lengths (Table II) which allow comparison to data obtained from dilute solution (see below).

Information of the stiffness of the modified xanthans in the ordered conformation can also be obtained from the relationship between $[\eta]$ and M_w. Since the chemical composition and, hence, the equivalent weight of the average repeating unit covary with the chain length, it

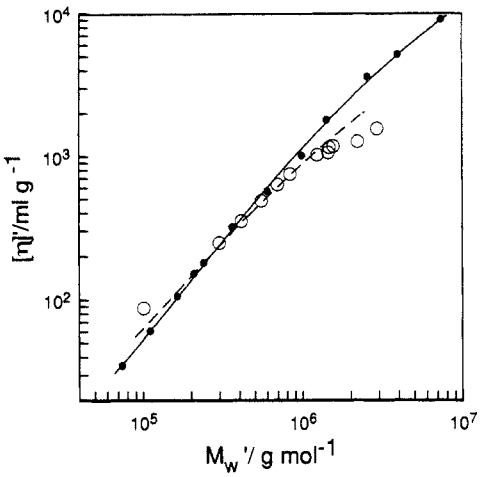

Figure 12. Double-logarithmic plot of $[\eta]'$ versus M_w' for the partially hydrolyzed xanthans (○, - - -). Literature data for sonicated xanthan fragments are included for comparison (●, —). Lines correspond to Yamakawa–Fuji–Yoshizaki theoretical curves (see text).

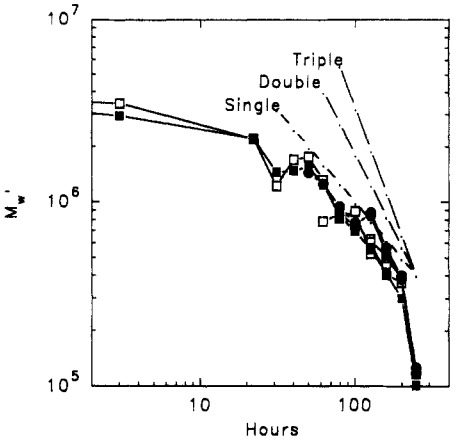

Figure 13. Double-logarithmic plot of M_w' versus t (hydrolysis time), using data from static light scattering measurements in 0.1 M NaCl (■) or 0.005 M NaCl (●) and HPLC–LALLS in 0.1 M NaCl (□). Lines (– · –) where the slopes are calculated by the Monte Carlo analysis[21] for single-, double-, and triple-stranded polymers have been included for comparison (see text).

becomes necessary to define an apparent or "hypothetical" molecular weight (M_w'), which corresponds to the molecular weight of depolymerized xanthans containing intact side chains (polypentamer) (eq 2). (The use of the weight-average degree of polymerization, DP_w,[18] would be an equivalent method to exclude the changes in the molar mass due to side-chain changes.) Further, an apparent intrinsic viscosity ($[\eta]'$) referring to constant chemical composition is defined (eq 3). Figure 12 shows a double-

$$M_w' = M_w[846/(324 + 360f_{ABA} + 162f_{\beta\text{-Man}})] \quad (2)$$

$$[\eta]' = [\eta][846/(324 + 360f_{ABA} + 162f_{\beta\text{-Man}})]^{-1} \quad (3)$$

logarithmic plot of M_w' and $[\eta]'$, using values calculated according to eqs 2 and 3, and with the corresponding $f_{\beta\text{-Man}}$ and f_{ABA} values taken from Table I. Below M_w values of 6.2×10^5 the data points fall on a straight line with a calculated slope of 1.0. Above this value a curvature is observed, which is at least partly ascribed to the effect on $[\eta]'$ due to shear thinning. The slope is smaller than the value 1.5 which is reported for sonicated xanthans (for $M_w < 2.5 \times 10^5$) by Sato and co-workers[10] and also lower than the value of 1.32 reported by Holzwarth[37] although the latter value is based only on two samples and is subject to a larger uncertainty.

The stiffness of xanthan can alternatively be characterized by means of the wormlike chain model.[38] In Figure 12 the values of $[\eta]'$ vs M_w' are compared to the experimental data reported by Sato.[12] The continuous and dashed lines depict the best fits to the $[\eta]'$ vs M_w' data using the wormlike chain model.[38] Note that the literature data are obtained for sonicated xanthans with intact side chains where M_w' therefore equals M_w and $[\eta]'$ equals $[\eta]$. The sum square of residuals between the data and the model were minimized using the simplex algorithm[39] treating the linear mass density, M_L, hydrodynamic diameter, d, and persistence length, q, as freely adjustable parameters. The parameters obtained for the $[\eta]$–M_w literature data[12] for this fit, $M_L' = 2075$ nm^{-1}, $d = 3.2$ nm, and $q = 105$ nm, are in good agreement with the original estimates provided by Sato,[12] thus confirming that our approach yields consistent results with their data. Our experimental data for the partially hydrolyzed xanthans appear to be qualitatively similar to those reported by Sato. There appear, however, to be differences in the chain stiffness. When the chain stiffness was estimated using the Yamakawa–Yoshizaki theory of $[\eta]'$ vs M_w', we did only take into account the molecular weight range from 3×10^5 to 1.5×10^6, because the higher ones are expected to show deviations from zero shear rate $[\eta]$ values due to the actual shear rate in the capillary viscometer. The sample with the lowest M_w' was excluded because of the significant oligomeric fraction of this sample. Using the constraint 1950 nm$^{-1} < M_L' < 2150$ nm^{-1} (since molecular weights have been recalculated to refer to the polypentamer and, therefore, constant M_L'), we found that the experimental data could adequately be described by the parameter values $M_L' = 1951$ nm^{-1}, $d = 3.9$ nm, and $q = 50$ nm (broken line, Figure 12). The q_{3D} data (Table II) suggest the reduction in chain stiffness has leveled off already for $M_w < 1.0 \times 10^6$, thus suggesting that the samples included in the analysis have the same flexibility. We chose to base this analysis on $[\eta]'$ vs M_w' rather than the directly experimentally determined values because it allows a direct comparison to the literature data. This finding suggest that the decreased chain stiffness identified in the analysis of the electron micrographs also can be seen in the relation between $[\eta]'$ and M_w' and, furthermore, that the estimates of q from the two methods are in reasonable agreement.

Having established that partially hydrolyzed xanthans retain their original conformation in aqueous solution, i.e., an extended, double-stranded structure, despite the large structural changes in the side chains, we may now return to the question of how the depolymerization kinetics depends on conformational effects, as predicted in eq 1. Figure 13 shows a double-logarithmic plot of M_w' versus t, where t is the hydrolysis time. The curve has the shape which is predicted by Monte Carlo simulations of the random depolymerization of double-stranded polymers.[21] Initially, a slow decrease in log M_w' is observed. This corresponds to the induction period[21] where scissions in the main chain of the double-stranded molecules are on average too far apart to invoke a significant decrease in the molecular weight. In the region where $\log[M_w'(t)/M_w'(t=0)]$ decreases below −1, the molecular weight decay occurs more rapidly. According to the Monte Carlo simulations,[21] a power law decay in M_w is expected when $M_w(t)/M_w(t=0)$ is smaller than 0.1. Such a degree of depolymerization is only obtained for samples 11–13. Between samples 11 and 12 an average slope of −1.5 (±0.1) is found, using M_w' data from static light scattering

measurements. This value is near the value of 1.66 which is predicted for double-stranded polymers.[21] Between samples 12 and 13 a much steeper curve is found (slope of approximately −5), indicating that processes other than strand disintegration also contribute to the observed reduction in M_w (see below).

The Monte Carlo analyses have so far been carried out assuming that all bonds in the glucan backbone are cleaved at the same rate, irrespective of their position in the molecule or the conformational state, and that the rate does not vary with time. The reaction is further assumed to be first order with respect to the concentration of glucose residues linked in the polymer backbone. Attempts were made to confirm this assumption by analyzing the amount of reducing ends in the nondialyzable fraction, but the colorimetric methods available lack the sensitivity that is needed to quantify the small amounts of reducing ends found in these samples, except in samples 8–13. After about 50–70 h the rate of formation of reducing ends seems to increase. However, as shown in Figure 6 the major portion of the reducing ends is found in the low molecular weight fraction. It is consequently not possible to quantify the amount of reducing ends in the high molecular weight fraction. We suggest, as a tentative explanation, that the rate of hydrolysis of the single-stranded regions that are exposed when the low molecular weight fragments are released from the double-stranded species have a higher rate of hydrolysis and that this in part explains the unexpectedly large molecular weight decrease from sample 12 to sample 13. It may also in part explain that the amount of free glucose formed apparently exceeds the number of reducing ends by a factor of about 3 (Figure 4). Extended hydrolysis in the relatively short disordered fragments will produce a substantial amount of dialyzable oligomers and monomers, which cannot be detected as reducing ends in the nondialyzable fraction. In addition, terminal glucose residues, especially at the nonreducing end, may be more rapidly hydrolyzed than internal residues.[40] However, this effect will not increase the content of reducing ends in the nondialyzable fraction. It may thus be concluded that the data presented in Figure 13 do not fulfill the criteria for the use of eq 1 over the entire M_w range, particularly since the depolymerization rate possibly depends upon the conformational state.

The multimodal molecular weight distributions (MWD) seen in the HPLC curves (Figure 5) is a feature which more strongly seems to support the findings that partially hydrolyzed xanthans are double-stranded in the ordered state. If the samples were single-stranded a continuous MWD (Kuhn distribution) was to be expected. In such a case the only species which to some extent might accumulate in the nondialyzable fraction (free sugars are dialyzable) is the trisaccharide GlcA-α-Man-Glc, which is the "end product" before the slow hydrolysis of the α-mannose is considered. Such compounds are not separated on the column and will elute in the salt peak. Peak C, which contains the major portion of low molecular weight fragments, is somewhat asymmetric and is clearly broader than the salt peak, indicating a heterogeneous and polydisperse population of low molecular weight fragments. Figure 6b also shows that fraction II in Figure 6a can be further depolymerized by cellulase, indicating that this fraction consists of oligomeric species rather than the minimum end product. The release of glucose-containing oligomers of the observed size distribution therefore points toward a release mechanism other than that expected for a single-stranded polymer and is in agreement with a double-stranded model.

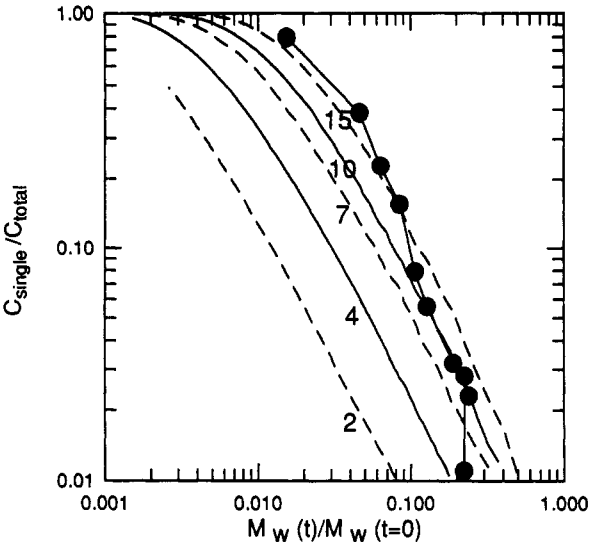

Figure 14. Relative amount of disordered fragments (C_{single}/C_{total}) as a function of the degree of depolymerization [expressed as $M_w(t)/M_w(t=0)$]. Symbols: experimental data. Lines: Monte Carlo simulations for DP_{min} = 2, 4, 7, 10, and 15 glucose residues.

The model for depolymerization of double-stranded polymers further predicts that any low molecular weight fragments released should be in the disordered state. Such fragments are too short to exist in the double-stranded, ordered conformation. The optical rotation data in Figure 7 clearly support the prediction in that the low molecular weight fraction, which has the same average sugar composition as the high molecular weight fraction, is in the disordered state at all temperatures. In contrast, the high molecular weight fraction undergoes the usual cooperative transition at T_m characteristic for xanthan.

According to the Monte Carlo analysis, the amount and MWD of the low molecular weight fragments depend on two factors other than the hydrolysis conditions, namely, the minimum length (DP_{min}) needed in order to stabilize an ordered structure and the number of broken bonds. The value of DP_{min} is of particular interest and represents the maximum number of glucose residues for any fragment which is released. Due to continued degradation the amount of fragments with DP = DP_{min} will be very low and cannot be detected. Figure 14 shows the Monte Carlo prediction of the relative amount of single-stranded fragments, C_{single}/C_{total}, released from a double-stranded polymer as a function of the degree of polymerization (represented as $[M_w(t)/M_w(t=0)]$ for several values of DP_{min}. This approach has an additional advantage, since variations in the depolymerization rate, which seem to occur here, do not influence the results. The experimental values for C_{single}/C_{total} (sum of peaks B and C divided by sum of peaks A–C; Figure 5) are shown on the same curve. The data seem to suggest that DP_{min} for the partially hydrolyzed xanthans is on the order of 10–15 glucose residues.

As an additional comment, the content of disordered fragments should have important effects on the values of ΔH_{cal} and $[\alpha]$, since they obviously cannot undergo an order–disorder transition. This comes in addition to the previously reported[19] dependency of ΔH_{cal} and $[\alpha]$ upon the composition of the side chains. However, the samples used in the previous study[19] had $[\eta]$ values in the region above 1000 mL g^{-1}, where C_{single}/C_{total} was less than 0.05. The reported quantitative relationships between ΔH_{cal} and $[\alpha]$ and the composition of the side chains therefore hold for the range of molecular weights studied previously. For more degraded samples corrections must be made.

The multimodal MWD of partially degraded xanthans supports the finding from electron microscopy concerning the double-stranded nature of the ordered conformation of xanthan. It also represents an alternative approach to obtain parameters governing the single- to double-stranded transition. Using the estimated DP_{min} in combination with the previously experimentally determined ΔH_{cal} and the cooperativity parameter σ,[19] the consistency of these transition parameters may in principle be evaluated. Although the available data for DP_{min}, ΔH_{cal}, and σ have been obtained for somewhat different solvent conditions, we note the apparently fair agreement between the present finding of DP_{min} in the range 10–15 glucose residues and our previously calculated value of 28 using ΔH_{cal} = 7.5 kJ mol^{-1} and $\gamma = \sigma c = 10^{-5}$.[17] The calculations were carried out using the nonstaggered zipper model for pairwise associating polymer chains, originally developed for DNA.[41] The value of ΔH_{cal} is within the experimentally determined range, whereas the selected value of σ would correspond to a fairly high polymer concentration. Despite these limitations, we would like to emphasize the nontrivial fact that the detailed analysis of the multimodal MWD obtained following partial hydrolysis of xanthan prove an alternative route to the study of parameters of the helix–coil transition.

Acknowledgment. This work was supported by VISTA (Grant V6314), a research cooperation between the Norwegian Academy of Science and Letters and Statoil and by the Royal Norwegian Council for Scientific and Industrial Research (NTNF) (Grant BT27472). M. Myhr and I. Mehli are thanked for skillful technical assistance.

References and Notes

(1) Kang, K. S.; Pettitt, D. J. In *Industrial Gums. Polysaccharides and Their Derivatives*; Whistler, R. L., BeMiller, J. N., Eds.; Academic Press: San Diego, 1993; pp 341–397.
(2) Conway, M. W.; Almond, S. W.; Briscoe, J. E.; Harris, L. E. *J. Pet. Technol.* **1983**, *Feb*, 315.
(3) Shu, P. *ACS Symp. Ser.* **1989**, *396*, 137.
(4) Nolte, H.; John, S.; Smidsrød, O.; Stokke, B. T. *Carbohydr. Polym.* **1992**, *18*, 243.
(5) Lund, T.; Smidsrød, O.; Stokke, B. T.; Elgsaeter, A. *Carbohydr. Polym.* **1988**, *8*, 245.
(6) Cheetham, N. W. H.; Mashimba, E. N. M. *Carbohydr. Polym.* **1991**, *14*, 17.
(7) Williams, P. A.; Day, D. H.; Langdon, M. J.; Phillips, G. O.; Nishinari, K. *Food Hydrocolloids* **1991**, *4*, 489.
(8) Atkins, E. *NATO ASI Ser., Ser. E* **1990**, *186*, 371.
(9) Sato, T.; Norisuye, T.; Fujita, H. *Polym. J.* **1985**, *17*, 729.
(10) Sato, T.; Kojima, S.; Norisuye, T.; Fujita, H. *Polym. J.* **1984**, *16*, 423.
(11) Sato, T.; Norisuye, T.; Fujita, H. *Polym. J.* **1984**, *16*, 341.
(12) Sato, T.; Norisuye, T.; Fujita, H. *Macromolecules* **1984**, *17*, 2696.
(13) Coviello, T.; Kajiwara, K.; Burchard, W.; Dentini, M.; Crescenzi, V. *Macromolecules* **1986**, *19*, 2826.
(14) Stokke, B. T.; Elgsaeter, A.; Smidsrød, O. *Int. J. Biol. Macromol.* **1986**, *8*, 217.
(15) Stokke, B. T.; Elgsaeter, A.; Smidsrød, O. *ACS Symp. Ser.* **1989**, *396*, 145.
(16) Stokke, B. T.; Smidsrød, O.; Elgsaeter, A. *Biopolymers* **1989**, *28*, 617.
(17) Kitamura, S.; Takeo, K.; Kuge, T.; Stokke, B. T. *Biopolymers* **1991**, *31*, 1243.
(18) Christensen, B. E.; Smidsrød, O. *Carbohydr. Res.* **1991**, *214*, 55.
(19) Christensen, B. E.; Knudsen, K. D.; Smidsrød, O.; Kitamura, S.; Takeo, K. *Biopolymers* **1993**, *33*, 151.
(20) Vanderslice, R. W.; Doherty, D. H.; Capage, M. A.; Betlach, M. R.; Hassler, R. A.; Henderson, N. M.; Ryan-Graniero, J.; Tecklenburg, M. In *Biomedical and Biotechnological Advances in Industrial Polysaccharides*; Crescenzi, V., Dea, I. C. M., Paoletti, S., Stivala, S. S., Sutherland, I. W., Eds.; Gordon and Breach: New York, 1989; pp 145–156.
(21) Stokke, B. T.; Christensen, B. E.; Smidsrød, O. *Macromolecules* **1992**, *25*, 2209.
(22) Thomas, C. A. *J. Am. Chem. Soc.* **1956**, *78*, 1861.
(23) Ash, S. G.; Clarke-Sturman, A. J.; Calvert, R.; Nisbet, T. M. *Soc. Petrol. Eng.* **1983**, paper 12085.
(24) Seright, R. S.; Henrici, B. J. *Soc. Petrol. Eng.* **1986**, paper 14946.
(25) Knutsen, S. H.; Moe, S. T.; Larsen, B.; Grasdalen, H. *Hydrobiologia* **1993**, *260/261*, 667.
(26) Lecourtier, J.; Chauveteau, G.; Muller, G. *Int. J. Biol. Macromol.* **1986**, *8*, 306.
(27) Slootmaekers, D.; van Dijk, J. A. P. P.; Varkevisser, F. A.; Bloys van Treslong, C. J.; Reynaers, H. *Biophys. Chem.* **1991**, *41*, 55.
(28) Stokke, B. T.; Elgsaeter, A.; Bjørnestad, E. O.; Lund, T. *Carbohydr. Polym.* **1992**, *17*, 209.
(29) Hodge, J. E.; Hofreiter, B. T. *Meth. Carbohydr. Chem.* **1962**, *1*, 386.
(30) Miller, G. L.; *Anal. Chem.* **1959**, *31*, 426.
(31) Filisetti-Cozzi, T. M. C. C.; Carpita, N. C. *Anal. Biochem.* **1991**, *197*, 157.
(32) Dubois, M.; Gilles, K. A.; Hamilton, J. K.; Rebers, P. A.; Smith, F. *Anal. Chem.* **1956**, *28*, 350.
(33) Tylor, J. M.; Branton, D. *J. Ultrastruct. Res.* **1980**, *71*, 95.
(34) Stokke, B. T.; Brant, D. A. *Biopolymers* **1990**, *30*, 1161.
(35) Paradossi, G.; Brant, D. A. *Macromolecules* **1982**, *15*, 874.
(36) Hacche, L. S.; Washington, G. E.; Brant, D. A. *Macromolecules* **1987**, *20*, 2179.
(37) Holzwarth, G. *Carbohydr. Res.* **1978**, *66*, 173.
(38) Yamakawa, H.; Yoshizaki, T. *Macromolecules* **1980**, *13*, 633.
(39) Caceci, M. S.; Cacheris, W. P. *Byte* **1984**, *May*, 340.
(40) BeMiller, J. N. *Adv. Carbohydr. Chem.* **1967**, *22*, 25.
(41) Applequist, J.; Damie, V. *J. Am. Chem. Soc.* **1965**, *87*, 1450.

Author Supplied Registry No. Xanthan gum, 11138-66-2.